

Thermo-mechanical analysis of additive manufacturing for material properties estimation of layered polymer composite

Bashir, U., Hassan, A., Ahmed, F., Mobeen, H., Zain-ul-abdein, M., Dildar, A., Hayat, Q., Ijaz, H., Asad, M. & Djavanroodi, F
Author post-print (accepted) deposited by Coventry University's Repository

Original citation & hyperlink:

Bashir, U, Hassan, A, Ahmed, F, Mobeen, H, Zain-ul-abdein, M, Dildar, A, Hayat, Q, Ijaz, H, Asad, M & Djavanroodi, F 2023, 'Thermo-mechanical analysis of additive manufacturing for material properties estimation of layered polymer composite', *Mechanics of Advanced Materials and Structures*, vol. (In-Press), pp. (In-Press).
<https://doi.org/10.1080/15376494.2023.2255258>

DOI 10.1080/15376494.2023.2255258

ISSN 1537-6494

ESSN 1537-6532

Publisher: Taylor and Francis

*This is an Accepted Manuscript version of the following article, accepted for publication in *Mechanics of Advanced Materials and Structures*. Bashir, U, Hassan, A, Ahmed, F, Mobeen, H, Zain-ul-abdein, M, Dildar, A, Hayat, Q, Ijaz, H, Asad, M & Djavanroodi, F 2023, 'Thermo-mechanical analysis of additive manufacturing for material properties estimation of layered polymer composite', *Mechanics of Advanced Materials and Structures*, vol. (In-Press), pp. (In-Press)..*

It is deposited under the terms of the Creative Commons Attribution-NonCommercial License (<http://creativecommons.org/licenses/by-nc/4.0/>), which permits non-commercial re-use, distribution, and reproduction in any medium, provided the original work is properly cited.

Thermo-Mechanical Analysis of Additive Manufacturing for Material Properties Estimation of Layered Polymer Composite

Usman Bashir ^a, Abrar Hassan ^a, Furqan Ahmed ^a, Muhammad Zain-ul-abdein ^{a,*},

Hajrah Mobeen ^a, Abdullah Dildar ^a, Qamar Hayat ^{b,c}, Hassan Ijaz ^d,

Muhammad Asad ^e, Faramarz Djavanroodi ^e

^a *Department of Metallurgical and Materials Engineering (MME), University of Engineering and Technology (UET), Lahore 54890, Pakistan.*

^b *Warwick Manufacturing Group, University of Warwick, Coventry, CV4 7AL, UK.*

^c *Institute for Clean Growth and Future Mobility, Coventry University, Coventry, CV1 5FB, UK.*

^d *School of Engineering, University of Leicester, Leicester LE1 7RH, UK.*

^e *Mechanical Engineering Department, Prince Mohammad Bin Fahd University, AL-Khobar 31952, Saudi Arabia.*

Abstract

This paper proposes a numerical approach for predicting residual stresses induced during the additive manufacturing (AM) of polymer composites and their effect on the deformation behavior of the composites. A finite element (FE) model was developed on Abaqus /Standard for 3D printing of layered polymer composite using three polymers: HDPE, PVC, and ABS. The material properties of pure polymers and their blends were measured through tensile testing of injection-molded specimens. These properties were then used as input data in the FE model for the regions of pure polymers and their interfaces. An uncoupled thermo-mechanical analysis was performed, where a heat transfer analysis was realized first using elements birth (activation /deactivation) technique and a moving cylindrical volumetric heat source as a Fortran subroutine (DFLUX). With temperature input from thermal simulation, a mechanical analysis was carried out to deform the

polymer composites along and across the print direction, i.e., under isostrain and isostress conditions, respectively. It was observed that the theoretical models existing in the literature underestimate the material properties as they do not consider the residual stresses developed during fabrication. The FE simulations predicted that the estimated material properties were 10 to 50% different from those calculated by the theoretical models, depending upon the residual stress level and the print direction.

Keywords: Additive Manufacturing; Polymer Composite; Finite Element Analysis; Isostrain; Isostress; Material Properties.

* Corresponding Author: M. Zain-ul-Abdein

Department of Metallurgical and Materials Engineering

University of Engineering and Technology, Lahore, Pakistan 54890

Tel.: +92 42 99029207; Fax: +92 42 99250202

Email: mzainulabdein@gmail.com

1. Introduction

Additive manufacturing (AM) has become a popular manufacturing technique in recent years due to its flexibility and ease of operation. It can be conveniently applied to 3D print plastics, metals, ceramics, concretes, and many other materials. In comparison with conventional forming methods, 3D printing has many advantages, including high precision, cost-effectiveness, minimum waste, and customized design [1]. Owing to the limited mechanical properties of 3D printed pure polymer parts, there is a need to develop high-performance printable polymer composites [2]. Techniques like fused deposition modeling (FDM), powder bed and inkjet head 3D printing, stereolithography (SLA), selective laser sintering (SLS), etc., are currently being used to print polymeric composites. Particle- and fiber-reinforced polymer composites, epoxy matrix composite and nanocomposites have been made and tested by many researchers using similar techniques [3-9].

Reinforced polymeric composites are widely used due to their low cost and improved mechanical properties [10-12]. It is a common practice to mix particles and fibers with polymers, either in powder form for SLS, or in liquid form for SLA, or for further extrusion into printable filaments for the FDM process [13,14]. Chung et al. [15] developed polymer-based composite of Nylon 11 by adding glass beads through SLS, which improved tensile modulus of the composite. Nikzad et al. [16] investigated the thermal and mechanical properties of FDM printed metal-particle-filled acrylonitrile butadiene styrene (ABS) composites. They found that an inclusion of iron/copper particles of up to 40 % shows a significant improvement in thermal and mechanical properties of the ABS. Melchels et al. [17] and Boparai et al. [18] fabricated Nylon 6-Al-Al₂O₃ particle reinforced composite using the FDM and reported improved wear resistance of Nylon 6. Isakov et al. [19] manufactured a polymer-based micro-ceramic composite with controlled permittivity and directly printed two different filaments having ABS only and an ABS + 30 vol.% Ba_{0.64}Sr_{0.36}TiO₃

through a dual-filament FDM technique. Zhong et al. [20] studied the effect of short glass fibers and plasticizer on various properties of ABS based 3D printed composite. Glass fibers significantly improved the strength of ABS filament but flexibility and handleability was reduced. Tian et al. [21] co-extruded PLA filaments and continuous carbon fibers and identified the effect of different parameters like deposition layer thickness, liquefier temperature, hatch spacing, and printing speed on the mechanical properties of the continuous fiber reinforced PLA composites. Lu et al. [22] analyzed shape memory polymer nanocomposite using carbon nanotube (CNT) and boron nitride and characterized their thermomechanical properties.

Addition of nanoparticles such as CNT, graphene, graphite, ceramic, and metal nanoparticles was found to yield significant improvement in mechanical, electrical, and thermal properties of 3D printed polymer composites in several studies [23-28]. For instance, an addition of 5 wt.% nano-titanium dioxide (TiO_2) [10], 10 wt.% carbon nanofibers [29], and 10 wt.% multi-walled CNT [30] showed a 13.2%, 39%, and 7.5% increase in the tensile strength of printed composite parts compared with the unfilled polymer parts, respectively. Tambrallimath and co-workers [31] developed filaments of polycarbonate (PC) and ABS by mixing them together and then extruding the blend through a 1.75 mm diameter nozzle of an FDM 3D printer. Their findings showed that good interfacial strength and presence of graphene in the blend improves elastic modulus of the polymeric composite.

Material property assessment of polymer blends printed through FDM is critical to their successful exploitation in various applications [32-36]. Mostly standard mechanical tests such as impact, tensile, and compression tests are realized for this purpose on 3D printed products [37-41]. The mechanical properties, however, vary greatly depending upon the printing parameters, including but not limited to melt temperature, interfacial strength, infill density, etc. In their works, Carrera

and Miguel [42-45] used FE analyses to model the stress behavior of layered composite structures. Although many research works have been published over the last couple of decades that are dedicated to the material properties characterization of 3D printed polymer layered composites, numerical models to predict these properties are still rare to be found in literature. In this work, a novel experimental and numerical approach is being proposed to estimate and predict the mechanical properties of 3D printed layered polymer composites along and across the print direction using 3 different polymers.

2. Materials and Methods

2.1. Modeling Approach

AM of a polymer composite through FDM requires the deposition of polymer layers next to each other. As each layer is printed in melt state, it fuses with the adjacent layer deposited previously, leading to the formation of an interfacial zone. This zone plays an important role in determining the overall properties of the material, particularly when the adjacent layers are of different polymers. [Figure 1](#) depicts a generalized 3D model of layered polymer composite that contains three different polymers, labeled as P1, P2 and P3. Furthermore, the interfacial zones between adjacent layers are represented as P1+P2, P2+P3 and P3+P1.

In the present work, three different polymers viz. high-density polyethylene (HDPE), polyvinyl chloride (PVC) elastomer and ABS, and their combinations were injection molded before performing mechanical testing. The material properties, so obtained, furnished the database for pure polymers and interfacial zones of the numerical model. Finite element (FE) simulations for 3D printing of the whole model ([Figure 1](#)) were performed to calculate thermal histories and the resulting residual stresses. The material properties of the printed model were then predicted by applying the stress along and across the print direction, i.e., under isostrain and isostress

conditions, respectively. For a two-phase fibre-matrix composite, a generalized form to estimate thermal and mechanical properties under the isostrain (along the fibre axis) and isostress (across the fibre axis) conditions may be stated as:

$$\phi_{composite}^{isostrain} = v_{fibre}\phi_{fibre} + v_{matrix}\phi_{matrix} \quad (1)$$

$$\phi_{composite}^{isostress} = \frac{\phi_{fibre}\phi_{matrix}}{v_{fibre}\phi_{matrix} + v_{matrix}\phi_{fibre}} \quad (2)$$

where, ϕ refers to the material property, such as thermal conductivity, elastic modulus, yield strength, etc., and v denotes the volume fraction. These equations may be modified to include more than two ingredients in a composite. However, they do not take into account the effect of residual stresses. Unlike the theoretical isostrain and isostress models (Eqs. (1) and (2)), the resulting simulated properties in the present investigation showed the effect of interfacial zones and thermal history experienced by the polymer composite during AM.

2.2. Experimental Work

Commercially available PVC elastomer, HDPE and ABS in granular form were used as raw materials to manufacture the tensile test specimens. The composition of the ‘as-received’ polymer powders was verified at first using a PerkinElmer-ATR instrument for Fourier transform infrared (FTIR) spectroscopy. The powders were scanned from 400 to 4000 cm^{-1} wavenumber at a rate of 2 mm/s and a resolution of 4 cm^{-1} . The FTIR results were compared to the standard curves of the polymers (see Figure 2).

A semi-automatic injection molding machine was used to prepare samples of pure polymer and polymer blends. Polymer powders of predetermined compositions were heated within the nozzle to a prescribed temperature. Upon reaching the desired temperature, the melt was injected through

the nozzle into a die placed underneath. [Figure 3](#) shows the schematics of the die-design and specimen geometry. A control circuit with a relay maintained the processing temperature during injection within an accuracy of $\pm 1^\circ\text{C}$, and a steady pressure was applied to ensure laminar flow of the polymer. The tensile test samples were retrieved from the die upon cooling. [Table 1](#) summarizes the compositions of the various polymer combinations and their corresponding processing temperatures. Polymer blends were prepared to identify the properties of interfaces between the respective polymers. Tensile tests for each composition were carried out on a 10 kN universal testing machine TIRAtest2810 (Schalkau, Germany). The machine was operated in the displacement mode, while the crosshead speed was maintained at 10 mm/min. Each test was conducted at least three times to ensure repeatability.

2.3. Finite Element Modeling

Commercially available FE software Abaqus /Standard was used to develop a 3D model of polymer composite (dimensions: 6 mm x 6 mm x 1 mm) as shown in [Figure 1](#). Polymer layers were added successively along the print direction in the form of element sets, each of size 1 mm x 1 mm x 1 mm. Each element set was activated using Abaqus's built-in 'Model Change' option. This requires all the elements to be deactivated at the beginning of the analysis and then activated at the prescribed time as determined by the printing speed. During activation thermal boundary conditions are also applied at the newly appearing surfaces that are exposed to the ambient.

The FE mesh consisted of 8 nodes 3D linear brick elements, namely DC3D8 and C3D8R for thermal and mechanical analyses, respectively. The smallest element size was 0.25 mm x 0.25 mm x 0.25 mm. Note that one fourth of the width of each polymer layer contributed to the interfacial zone, where two adjacent layers were assumed to create a polymer blend of 50 vol. % of each polymer. It is to be mentioned that the choice of element size is dependent on the application of

the heat source such that each activating element set appears at melt temperature. Increasing mesh density beyond this point would lead to increase in computation time without any appreciable difference in the results.

Since mechanical dissipation involved in AM is too little to generate any appreciable amount of heat, a sequentially coupled temperature-displacement analysis was deemed sufficient to obtain residual stress state in the printed composite model. Once the pre-stressed state was achieved, a uniaxial stress was applied in the plane of the specimen under the isostress and isostrain conditions.

2.3.1. Heat Transfer Analysis

Heat transfer analysis was performed initially to identify the heat source parameters and the corresponding transient temperature (T) distribution in space (x, y, z) and time (t). This requires the solution of the following equation:

$$\frac{\partial}{\partial x} \left(k \frac{\partial T}{\partial x} \right) + \frac{\partial}{\partial y} \left(k \frac{\partial T}{\partial y} \right) + \frac{\partial}{\partial z} \left(k \frac{\partial T}{\partial z} \right) + Q_v = \rho C_p \left(\frac{\partial T}{\partial t} \right) \quad (3)$$

where, k, ρ , C_p , and Q_v are the thermal conductivity ($\text{W.m}^{-1}.\text{K}^{-1}$), density (kg.m^{-3}), specific heat capacity ($\text{J.kg}^{-1}.\text{K}^{-1}$) and the volumetric heat flux (W.m^{-3}), respectively. Since FDM involves deposition of polymer melt on the printer platform that subsequently solidifies at room temperature, a volumetric heat source travelling on top of the activating element sets at the printing speed must be modeled to ensure the addition of elements at melt temperature. Such a movable heat source can be programmed as a Fortran subroutine, called DFLUX. Solidification / cooling of the printed specimen generally takes place in the air, hence a heat transfer coefficient for free convection ($\sim 10 \text{ W.m}^{-2}.\text{K}^{-1}$) needs to be applied at the surfaces exposed to the ambience.

2.3.2. Heat Source Model

For applications similar to AM, such as welding, several heat source models, ranging from conical to spherical to double-ellipsoidal, exist in the literature [46-48] that can successfully apply moving volumetric heat flux (Q_v). During welding, however, the heat flux distribution differs from that of AM in a way that it assumes maximum heat flux at the top surface while decreasing heat intensity in the thickness direction. FDM based AM, on the other hand, introduces droplets of molten material, wherein it is safe to assume that the heat distribution remains constant at the time of deposition. This necessitates programming of a cylindrical, rather than a conical or ellipsoidal, distribution of heat flux in the thickness direction. Figure 4 presents the schematics of one such heat source, adopted from [49]. The volumetric heat flux (Q_v) with Gaussian distribution may be evaluated in cylindrical coordinates as:

$$Q_v = \int_{z_i}^{z_e} \int_0^{2\pi} \int_0^{r_c} Q_o \exp\left(-\frac{3r^2}{r_c^2}\right) r \, dr \, d\theta \, dz \quad (4)$$

where, Q_o is the maximum heat flux (W) that is proportional to the peak temperature reached during 3D printing, r_c is the parameter for the flux distribution within the cylindrical region as a function of height (z), and r is the current radius within the xy-plane. Solution of the eq. (4) gives,

$$Q_v = Q_o \cdot \frac{9 \exp(3)}{\pi(\exp(3)-1)} \cdot \frac{1}{(z_e-z_i)(r_e^2+r_e r_i+r_i^2)} \exp\left(-\frac{3r^2}{r_c^2}\right) \quad (5)$$

With, $r_c = r_i + (r_e - r_i) \frac{z-z_i}{z_e-z_i}$

Here, the parameters r_e and r_i are the radii at the top and bottom of the cylinder at the locations z_e and z_i , respectively. While the height ($z_e - z_i$) of the cylindrical zone is equal to the thickness of the elements layer, r_e and r_i may be adjusted to ensure uniform temperature at the beginning of the deposition.

2.3.3. Stress analysis

The thermal history calculated during the heat transfer simulation was read by the mechanical analysis as a predefined field. The material properties were assumed to have an elastic-perfectly-plastic behavior, where the total strain (ε) may be represented as a combination of elastic (ε^e), plastic (ε^p) and thermal (ε^t) strains.

$$\varepsilon = \varepsilon^e + \varepsilon^p + \varepsilon^t \quad (6)$$

The elastic strain (ε^e) tensor in Eq. (6) is related to the stress (σ) tensor through a compliance (\mathbf{S}) tensor as $\varepsilon^e = \mathbf{S} : \sigma$; where \mathbf{S} depends upon the material's Young's modulus (E) and the Poisson's ratio (ν). The plastic term (ε^p) is defined by the yield function (f) such that $f(\sigma) < 0$, where $\sigma = \sigma_y$ is the material's yield strength. Finally, the thermal strain (ε^t) is determined by the thermal expansion coefficient (α) and a reference temperature (T_o).

Finally, it was assumed that the deposition of consecutive polymer layers produced polymer blend at the interfaces, and hence, a perfect contact was modeled between the layers. This allowed modeling of the whole composite as a single 'part' in Abaqus with different material properties in different regions without the need for contact formulation, thereby saving considerable computation time.

3. Results and Discussions

3.1. Mechanical Properties

Figure 5 compares elastic modulus, yield strength, and tensile strength of HDPE, ABS, and PVC elastomer in various combinations. For example, Fig 5a demonstrates difference in properties between HDPE and ABS, as well as a 50 vol. % combination of both. Likewise, Figs. 5b and 5c

represent the comparison between ABS-PVC and PVC-HDPE, respectively. [Figure 5d](#) shows the sequence of the layers in which different polymers would be printed. Notice that the 50 vol. % combinations of polymers furnish the properties of the interfaces between the corresponding adjacent polymers. It may be observed that ABS, being the stiffest and strongest of all the materials, is likely to increase the overall strength of the material. On the other hand, PVC elastomer, being the least stiff and having low strength, is expected to enhance the ductility of the printed composite. Additionally, the interface material with intermediate properties of the adjacent polymers may serve the purpose of a smooth transition of stresses and strains across the interface, which, in turn, can prevent sudden sharp increase in stresses and corresponding catastrophic failure due to stress raisers. It is worth mentioning that these interfacial properties were determined experimentally with the help of injection molded tensile test specimens, and hence, the 50 vol. % composite samples behaved as homogeneous materials and depicted no effect of directionality. Estimating these properties using isostrain and isostress formulations from [equations \(1\) and \(2\)](#), respectively, could have led to a significant difference in material properties, which might also have influenced the numerical simulation results.

3.2. Printing Simulation

3D printing in Abaqus is typically accomplished by time-dependent activation and deactivation. [Figure 6](#) illustrates activation / element birth of cube-shaped element sets of HDPE, PVC, and ABS layers starting from an initially deactivated 3D model. A second set of HDPE, PVC and ABS layers was deposited in the same manner to ensure the presence of ABS and HDPE next to each other, and in the middle of the specimen. The direction of elements birth indicates the printing direction and the direction of the heat source movement through the DFLUX subroutine. It is noteworthy that the heat source ‘hot spot’ is always present at the location of the newly born

element set, which confirms that the rate at which the heat source advances is identical to the printing speed. Additionally, it should also be noted that the peak temperature of the hot spot never exceeds 200 °C, which is in fact the print temperature where all the polymers would be in melt state (see [Table 1](#)). Furthermore, the through-thickness temperature distribution shows negligible difference in temperatures. This observation is consistent with the cylindrical distribution of the volumetric heat flux. Cooling of the printed specimen in reality varies greatly in the thickness direction because of the difference in heat loss by conduction through the printing platform and by convection in the air. In the current model, however, only the effect of free convection in the air on all surfaces is visible from the temperature contours of [Figure 6](#). It may be observed that the deposition of each next layer preheats the previous adjacent layer to a temperature as high as 100 °C, which is high enough to cause considerable repeated expansion and contraction. This is the source of residual stresses in 3D printed parts, and the effect is even more pronounced when a heterogeneous polymer composite is printed due to the difference in thermal expansion coefficients.

3.3. Thermal Histories

[Figure 7](#) demonstrates the temperature vs. time curve for the very first layer of HDPE. A total of 6 cube-shaped element sets were deposited during the first 6 seconds of the simulation run. Although the ‘birth’ temperature of each element set was maintained at 200 °C, yet it surpassed to as high as 220 °C at the beginning of the analysis for the first element set due to excessive heat flux accumulation and no active cooling surface for convection to be effective. For all other element sets from the second to the sixth, however, the initial temperature remained at the prescribed temperature of 200 °C. As soon as the heat source moved to the second element set, cooling of the first set started immediately since its newly activated surfaces were then exposed to

the ambient temperature. Similarly, when the heat source advanced, more element sets appeared, and the number of external surfaces kept on increasing. This led to a rapid drop in temperature as the newer elements experienced quenching in air and conduction with trailing colder elements. Once the deposition of elements was complete, further decrease in temperature was only a consequence of heat transfer in the surrounding due to free convection.

It may be noticed that the cooling curve showed serrations even after the deposition of the complete layer. This was simply a numerical approximation during the addition of subsequent layers of ABS and PVC elastomer. It is at this point conceivable that the subsequent layers would experience a similar cooling pattern for cooling is a surface phenomenon dependent upon the initial and sink temperatures as well as the heat transfer coefficient, and not the intrinsic material properties. Since all these factors are identical for the subsequent layers, no noticeable difference in the cooling rate was observed.

3.4. Residual Stresses

The heating and cooling cycles experienced by the polymer composite model are not the only sources of residual stresses during AM. There are, in fact, two additional sources of induced residual stresses in the model under investigation. The first of these is the difference in material properties of the adjacent layers, while the second one is the activation / deactivation of the element sets being printed. Although the material properties remain present throughout the analysis, they are only activated when the corresponding elements are born. The element set that appears at the beginning of the analysis experiences more heating / cooling cycles due to heat conduction within the model from the moving heat source and the heat loss in the surrounding compared to the one born towards the end of analysis. Therefore, the first element set has got the longest thermal history relative to the last one and is expected to have a different stress level.

Figure 8 illustrates contours of the longitudinal (along the print direction) residual stress and their distribution on the top surface in the transverse direction. Similar to the residual stresses induced during welding [50], the AM also yields maximum stress level along the direction of the heat source movement, while all other stress components remain trivial. The longitudinal residual stress is also plotted as a function of transverse distance in Fig 8. It can be observed that both the tensile and compressive zones exist across the length. However, a relatively smooth transition in stress distribution was noticed instead of a discontinuous change at the interface. Figure 8 also indicates that the maximum tensile and minimum compressive residual stresses are present within first three layers of HDPE, PVC, and ABS, from 0 to 3 mm, yet a lower level of stresses was recorded, from 3 to 6 mm, within the next three layers of the same combination of polymers. This is consistent with the above discussed phenomenon that the material deposited earlier experiences repeated heating and cooling during the process, and is, therefore, prone to higher level of residual stresses. Nevertheless, the nature of these stresses, tensile or compressive, did not change for the same material, i.e., tensile stresses in HDPE and ABS, and compressive stresses in PVC. It is evident that changing the polymers as well as the sequence of layers will influence the stress distribution, but a complete absence of residual stresses is out of the question.

3.5. Isostrain and Isostress Properties

The isostrain and isostress conditions applied to the prestressed 3D printed model are shown schematically in Figure 9. It should be pointed out that the isostrain condition, where stress is applied along the print direction, gives maximum stiffness and strength values. On the contrary, the isostress condition with stress applied across the print direction results in a minimum value of elastic modulus and yield and tensile strengths. Figure 9 demonstrates the theoretical true stress-true strain curves for isostrain and isostress conditions, obtained from equations (1) and (2),

respectively, for equal volume fractions of HDPE, ABS and PVC. These curves are frequently referred to as upper and lower bounds in the literature, or Wiener bounds after [51], as they determine the envelope of possible values of material properties for a given material. However, Wiener bounds do not consider any residual stresses that may have developed in a composite sample during manufacturing.

Recall that the samples of HDPE, PVC, and ABS blend containing 33.3 vol. % of each, were also injection-molded and tested to obtain the stress-strain response of a composite with equal volume fraction. The curve highlighted as an experimental result in Fig 9 represents this composite. Given that the equal volume fraction composite samples were injection-molded from powdered state, they were expected to behave like isotropic material with a stress-strain curve lying midway within the Wiener bounds. Although the experimental results do not appear to favor either the upper or lower bound, the curve seems to be reflecting degradation of the strength values in particular. For instance, the maximum experimental tensile strength of almost 8 MPa was closer to the theoretical minimum tensile strength of 5 MPa than the theoretical maximum of 22 MPa. A possible reason for this behavior could be associated with some other factor such as degree of crystallinity, which could be improved by merely controlling the cooling rate of the sample. However, this discussion is beyond the scope of the current investigation.

Figure 9 also compares the envelope of theoretical stress-strain curves with those obtained from FE simulations. It should be noted that FE simulated curves also include both the isostrain and isostress cases, and therefore, develop an envelope of their own that apparently underestimates the theoretical curves. The reason for this difference is quite obvious from the above discussion, where it was argued that the presence of residual stresses would influence the stress-strain behavior of the layered composite. It is clear from Fig 9 that the simulated and theoretical isostrain curves do

not differ significantly, at least during the elastic deformation. The maximum tensile strength, however, was almost 10% more for the former than for the latter. The effect of residual stress on the simulated and theoretical curves was found to be more pronounced for the isostress conditions. The FE simulations predicted 50% lower elastic modulus and the tensile strength of the layered composite relative to the theoretical lower bound. This may be justified based on the longitudinal stress distribution (see [Figure 8](#)). As the longitudinal stresses were predominant during the mechanical simulation, the model showed more resistance to deformation along the print direction leading to somewhat higher level of tensile strength. Across the print direction, however, the longitudinal stresses had little to no role to play in improving the strength. Instead, the discontinuity in the material properties coupled with residual stresses across the interface led to a quick elastic and plastic deformation of the composite, thereby resulting in smaller values of elastic modulus, and tensile strength.

4. Conclusions

With the aim of evaluating stress-strain behavior of 3D printed layered polymer composite under isostrain and isostress conditions, uncoupled thermo-mechanical analysis was performed. The following conclusions can be drawn:

- Theoretical models to calculate the elastic modulus, yield strength and tensile strength of polymer composite have the tendency to underestimate the deformation behavior.
- To accurately predict the stress-strain behavior of the polymer composite, the residual stresses developed during fabrication may not be ignored.
- AM-induced longitudinal residual stresses play a significant role in determining the mechanical properties of the composite along and across the print directions.

- The proposed FE modelling and simulation approach can help predict the structural integrity of 3D printed parts, and tailor the characteristics of finished printed components with respect to the combination, sequence, and directionality of polymeric materials.

Acknowledgments

The authors would like to acknowledge the Higher Education Commission, Islamabad – Pakistan, for its support in this work under National Research Program for Universities (NRPU) Project no. 16531 (Ref No. 20-16531/NRPU/R&D/HEC/2021 dated 29.04.2022).

Declaration of interest statement

The authors declare that there are no competing interests.

References

1. B.P. Conner, G.P. Manogharan, A.N. Martof, L.M. Rodomsky, C.M. Rodomsky, D.C. Jordan, and J.W. Limperos, "Making sense of 3-D printing: Creating a map of additive manufacturing products and services," *Addit. Manuf.*, vol. 1-4, pp. 64- 76, Oct. 2014. DOI: 10.1016/j.addma.2014.08.005.
2. B. Utela, D. Storti, R. Anderson, M. Ganter, "A review of process development steps for new material systems in three dimensional printing (3DP)," *J. Manuf. Processes*, vol. 10, no.2, pp. 96- 104, Jul. 2008. DOI: 10.1016/j.jmapro.2009.03.002.
3. M. Pecora, O. Smerdova, and M. Gigliotti, "In-situ characterization of the local mechanical behaviour of polymer matrix in 3D carbon fiber composites by cyclic indentation test," *Compos. Struct.*, vol. 224, pp. 112268, Jul. 2020. DOI: 10.1016/j.compstruct.2020.112268.
4. D. Sharma, and S.S. Hiremath, "Additively manufactured mechanical metamaterials based on triply periodic minimal surfaces: Performance, challenges, and application," *Mech. Adv. Mater. Struct.*, vol. 29, no. 26, pp. 5077-5107, 2022, DOI: 10.1080/15376494.2021.1948151.
5. X. Wang, M. Jiang, Z. Zhou, J. Gou, and D. Hui, "3D printing of polymer matrix composites: A review and prospective," *Composites, Part B*, vol. 110, pp. 442- 458, Feb. 2017. DOI: 10.1016/j.compositesb.2016.11.034.
6. A.K. Sood, R.K. Ohdar, and S.S. Mahapatra, "Parametric appraisal of mechanical property of fused deposition modelling processed parts," *Mater. Des.*, vol. 31, no. 1, pp. 287- 295, Jan. 2010. DOI: 10.1016/j.matdes.2009.06.016.
7. V.C. Gavali, P.R. Kubade, and H.B. Kulkarni, "Property Enhancement of Carbon Fiber Reinforced Polymer Composites Prepared by Fused Deposition Modeling," *Mater. Today*, vol. 23, no. 2, pp. 221- 229, 2020. DOI: 10.1016/j.matpr.2020.02.020.

8. S. Khosravani, M.H. Sadr, E. Carrera, and A Pagani “Synthesis, experimental testing and multi-scale modelling of graphene foam/epoxy composite,” *Mech. Adv. Mater. Struct.*, vol. 30, no. 12, pp. 2477-2486, 2023. DOI: 10.1080/15376494.2022.2055242.
9. R. Brighenti, L. Marsavina, M.P. Marghitas, M.P. Cosma, and M. Montanari, “Mechanical characterization of additively manufactured photopolymerized polymers,” *Mech. Adv. Mater. Struct.*, vol. 30, no. 9, pp. 1853-1864, 2023, DOI: 10.1080/15376494.2022.2045655.
10. A.R.T. Perez, D.A. Roberson, and R.B. Wicker, “Fracture Surface Analysis of 3D-Printed Tensile Specimens of Novel ABS-Based Materials,” *J. Fail. Anal. Prev.*, vol. 14, pp. 343-353, Mar. 2014. DOI: 10.1007/s11668-014-9803-9.
11. P. Striemann, D. Huelsbusch, M. Niedermeier, and F. Walther, “Application-oriented assessment of the interlayer tensile strength of additively manufactured polymers,” *Addit. Manuf.*, vol. 46, pp. 102095, Oct. 2021. DOI: 10.1016/j.addma.2021.102095.
12. E.J. Ekoi, A.N. Dickson, and D.P. Dowling, “Investigating the fatigue and mechanical behaviour of 3D printed woven and nonwoven continuous carbon fibre reinforced polymer (CFRP) composites,” *Composites, Part B*, vol. 212, pp. 108704, May. 2021. DOI: 10.1016/j.compositesb.2021.108704.
13. F. Ning, W. Cong, J. Qiu, J. Wei, and S. Wang, “Additive manufacturing of carbon fiber reinforced thermoplastic composites using fused deposition modeling,” *Composites, Part B*, vol. 80, pp. 369- 378, Oct. 2015. DOI: 10.1016/j.compositesb.2015.06.013.
14. Z.C. Kennedy, and J.F. Christ , “Printing polymer blends through in situ active mixing during fused filament fabrication,” *Addit. Manuf.*, vol. 36, pp. 101233, Dec. 2020. DOI: 10.1016/j.addma.2020.101233.

15. H. Chung, and S. Das, "Processing and properties of glass bead particulate-filled functionally graded Nylon-11 composites produced by selective laser sintering," *Mater. Sci. Eng., A*, vol. 437, no. 2, pp. 226- 234, Nov. 2006. DOI: 10.1016/j.msea.2006.07.112.
16. M. Nikzad, S.H. Masood, and I. Sbarski, "Thermo-mechanical properties of a highly filled polymeric composites for Fused Deposition Modeling," *Mater. Des.*, vol. 32, no. 6, pp. 3448-3456, Jun. 2011. DOI: 10.1016/j.matdes.2011.01.056.
17. F.P.W. Melchels, J. Feijen, and D.W. Grijpma, "A review on stereolithography and its applications in biomedical engineering," *Biomater.*, vol. 31, no. 24, pp. 6121- 6130, Aug. 2010. DOI: 10.1016/j.biomaterials.2010.04.050
18. K. Boparai, R. Singh, and H. Singh, "Comparison of tribological behaviour for Nylon6-Al₂O₃ and ABS parts fabricated by fused deposition modelling," *Virtual Phys. Prototyping*, vol. 10, no. 2, pp. 56- 66, Mar. 2015. DOI: 10.1080/17452759.2015.1037402.
19. D.V. Isakov, Q. Lei, F. Castles, C.J. Stevens, C.R.M. Grovenor, and P.S. Grant, "3D printed anisotropic dielectric composite with meta-material features ," *Mater. Des.*, vol. 93, pp. 423-430, Mar. 2016. DOI: 10.1016/j.matdes.2015.12.176.
20. W. Zhong, F. Li, Z. Zhang, L. Song, and Z. Li, "Short fiber reinforced composites for fused deposition modeling," *Mater. Sci. Eng., A*, vol. 301, no. 2, pp. 125- 130, Mar. 2001. DOI: 10.1016/S0921-5093(00)01810-4.
21. X. Tian, T. Liu, C. Yang, Q. Wang, and D. Li, "Interface and performance of 3D printed continuous carbon fiber reinforced PLA composites," *Composites, Part A*, vol. 88, pp. 198-205, Sep. 2016. DOI: 10.1016/j.compositesa.2016.05.032.
22. H. Lu, Y. Yao, W.M. Huang, J. Leng, and D. Hui, "Significantly improving infrared light-induced shape recovery behavior of shape memory polymeric nanocomposite via a synergistic

- effect of carbon nanotube and boron nitride,” *Composites, Part B*, vol. 62, pp. 256- 261, Jun. 2014. DOI: 10.1016/j.compositesb.2014.03.007.
23. X. Yan, J. Gu, G. Zheng, J. Guo, A.M. Galaska, J. Yu, M.A. Khan, L. Sun, D.P. Young, Q. Zhang, S. Wei, and Z. Guo, “Lowly loaded carbon nanotubes induced high electrical conductivity and giant magnetoresistance in ethylene/1-octene copolymers,” *Polym.*, vol. 103, pp. 315- 327, Oct. 2016. DOI: 10.1016/j.polymer.2016.09.056.
24. K. Refai, M. Montemurro, C. Brugger, and N. Sainter, “Determination of the effective elastic properties of titanium lattice structures,” *Mech, Adv. Mater. Struct.*, vol. 27, no. 23, pp. 1966–1982, 2020. DOI: 10.1080/15376494.2018.1536816.
25. S. Berretta, R. Davies, Y.T. Shyng, Y. Wang, and O. Ghita, “Fused Deposition Modelling of high temperature polymers: Exploring CNT PEEK composites,” *Polym. Test.*, vol. 63, pp. 251- 262, Oct. 2017. DOI: 10.1016/j.polymertesting.2017.08.024.
26. L. Gorjan, R. Tonello, T. Sebastian, P. Colombo, and F. Clemens, “Fused deposition modeling of mullite structures from a preceramic polymer and γ -alumina,” *J. Eur. Ceram. Soc.*, vol. 39, no. 7, pp. 2463- 2471, Jul. 2019. DOI: 10.1016/j.jeurceramsoc.2019.02.032.
27. M.A. Ryder, D.A. Lados, G.S. Iannacchione, and A.M. Peterson, “Fabrication and properties of novel polymer-metal composites using fused deposition modeling,” *Compos. Sci. Technol.*, vol. 158, pp. 43- 50, Apr. 2018. DOI: 10.1016/j.compscitech.2018.01.049.
28. G. Mantegna, C. R. Vindigni, S. Valvano, A. Esposito, D. Tumino, A. Alaimo and C. Orlando, “Representative volume element homogenisation approach to characterise additively manufactured porous metals,” *Mech. Adv. Mater. Struct.*, vol. 30, no. 5, pp. 1073-1082, 2023, DOI: 10.1080/15376494.2022.2124002

29. H. Zhan, F. Cheng, Y. Chen, K.W. Wong, J. Mei, D. Hui, W.M. Lau, Y. Liu, "Transfer printing for preparing nanostructured PDMS film as flexible SERS active substrate," *Composites, Part B*, vol. 84, pp. 222- 227, Jan. 2016. DOI: 10.1016/j.compositesb.2015.08.080.
30. J.H. Sandoval, and R.B. Wicker, "Functionalizing stereolithography resins: effects of dispersed multi-walled carbon nanotubes on physical properties," *Rapid Prototyping J.*, vol. 12, no. 5, pp. 1355-2546, Oct. 2006. DOI: 10.1108/13552540610707059.
31. V. Tambrallimath, R. Keshavamurthy, S. D, P.G. Koppad, and G.S. Pradeep Kumar, "Thermal behavior of PC-ABS based graphene filled polymer nanocomposite synthesized by FDM process," *Compos. Commun.*, vol. 15, pp. 129- 134, Oct. 2019. DOI: 10.1016/j.coco.2019.07.009.
32. A. Bagheri, M.S.A. Parast, A. Kami, M. Azadi, and V. Asghari, "Fatigue testing on rotary friction-welded joints between solid ABS and 3D-printed PLA and ABS," *Eur. J. Mech. A. Solids*, vol. 96, pp. 104713, Nov-Dec. 2022. DOI: 10.1016/j.euromechsol.2022.104713.
33. V. Shanmugam, O. Das, K. Babu, U. Marimuthu, A. Veerasimman, D.J. Johnson, R.E. Neisiany, M.S. Hedenqvist, S. Ramakrishna, and F. Berto, "Fatigue behaviour of FDM-3D printed polymers, polymeric composites and architected cellular materials," *Int. J. Fatigue*, vol. 143, pp. 106007, Feb. 2021. DOI: 10.1016/j.ijfatigue.2020.106007.
34. M. Özenç, T. Tezel, and V. Kovan, "Investigation into impact properties of adhesively bonded 3D printed polymers," *Int. J. Adhes. Adhes.*, vol. 118, pp. 103222, Oct. 2022. DOI: 10.1016/j.ijadhadh.2022.103222.

35. M.E. Spreeman, H.A. Stretz, and M.D. Dadmun, "Role of compatibilizer in 3D printing of polymer blends," *Addit. Manuf.*, vol.27, pp. 267-277, May. 2019. DOI: 10.1016/j.addma.2019.03.009.
36. T.O. Tang, S. Holmes, B.J. Boyd, and G.P. Simon, "Extrusion and 3D printing of novel lipid-polymer blends for oral drug applications," *Biomater. Adv.*, vol. 137, pp. 212818, Jun. 2022. DOI: 10.1016/j.bioadv.2022.212818.
37. A.A.B. AbuBakar, M.Z.B. Zainuddin, A.N.B. Adam, I. S.B.M. Noor, N.B. Tamchek, M.S.B. Alauddin, and M.I.B.M. Ghazali, "The study of mechanical properties of poly(lactic) acid PLA-based 3D printed filament under temperature and environmental conditions," *Mater. Today*, vol. 67, pp. 652- 658, 2022. DOI: 10.1016/j.matpr.2022.06.198.
38. R.Torre, and S. Brischetto, "Experimental characterization and finite element validation of orthotropic 3D-printed polymeric parts," *Int. J. Mech. Sci.*, vol. 219, pp. 107095, Apr. 2022. DOI: 10.1016/j.ijmecsci.2022.107095.
39. T. Tezel, M. Ozenc, and V. Kovan, "Impact properties of 3D-printed engineering polymers," *Mater. Today Commun.*, vol. 26, pp. 102161, Mar. 2021. DOI: 10.1016/j.mtcomm.2021.102161.
40. J. Nomani, D. Wilson, M. Paulino, and M.I. Mohammed, "Effect of layer thickness and cross-section geometry on the tensile and compression properties of 3D printed ABS," *Mater. Today Commun.*, vol. 22, pp. 100626, Mar. 2020. DOI: 10.1016/j.mtcomm.2019.100626.
41. H. Jiang, H. Ziegler, Z. Zhang, H. Meng, D. Chronopoulos, and Y. Chen, "Mechanical properties of 3D printed architected polymer foams under large deformation," *Mater. Des.*, vol. 194, pp. 108946, Sep. 2020. DOI 10.1016/j.matdes.2020.108946

42. E. Carrera, A.G. Miguel, M. Filippi, I. Kaleel, A. Pagani, M. Petrolo, and E. Zappino, "Global-local plug-in for high-fidelity composite stress analysis in ABAQUS," *Mech. Adv. Mater. Struct.*, vol. 28, no. 14, pp. 1445-1450, 2021. DOI: 10.1080/15376494.2019.1676938.
43. E. Carrera, A.G. Miguel, M. Filippi, I. Kaleel, A. Pagani, M. Petrolo, and E. Zappino, "Global-local plug-in for high-fidelity composite stress analysis in Femap/NX Nastran," *Mech. Adv. Mater. Struct.*, vol. 28, no. 11, pp. 1121-1127, 2021. DOI: 10.1080/15376494.2019.1655689.
44. E. Carrera, M. Petrolo, M.H. Nagaraj, and M. Delicata, "Evaluation of the influence of voids on 3D representative volume elements of fiber-reinforced polymer composites using CUF micromechanics," *Compos. Struct.*, vol. 254, pp. 112833, 2020. DOI: 10.1016/j.compstruct.2020.112833
45. A.G. Miguel, I. Kaleel, M.H. Nagaraj, A. Pagani, M. Petrolo, and E. Carrera, "Accurate evaluation of failure indices of composite layered structures via various FE models," *Compos. Sci. Technol.*, vol. 167, pp. 174-189, Oct. 2018. DOI: 10.1016/j.compscitech.2018.07.031
46. J. Goldak, A. Chakravarti, and M. Bibby, "A new finite element model for welding heat sources," *Metall. Trans. B*, vol. 15, pp. 299- 305, 1984. DOI: 10.1007/BF02667333.
47. M. Zain-ul-abdein, D. Nelias, J.F. Jullien, and D. Deloison, "Prediction of laser beam welding-induced distortions and residual stresses by numerical simulation for aeronautic application," *J. Mater. Process. Technol.*, vol. 29, pp. 2907-2917, 2009. DOI: 10.1016/j.jmatprotec.2008.06.051.
48. P. Ferro, A. Zambon, F. Bonollo, "Investigation of electron-beam welding in wrought Inconel 706—experimental and numerical analysis," *Mater. Sci. Eng. A*, vol. 392, no. 1-2, pp. 94- 105, 2005. DOI: 10.1016/j.msea.2004.10.039.

49. M. Zain-ul-abdein, D. Nélías, J.F. Jullien, and D. Deloison, “Experimental investigation and finite element simulation of laser beam welding induced residual stresses and distortions in thin sheets of AA 6056-T4,” *Mater. Sci. Eng., A*, vol. 527, pp. 3025- 3039, 2010. DOI: 10.1016/j.msea.2010.01.054.
50. M. Zain-ul-abdein, D. Nélías, J.F. Jullien, F. Boitout, L. Dischert, and X. Noe, “Finite element analysis of metallurgical phase transformations in AA 6056-T4 and their effects upon the residual stress and distortion states of a laser welded T-joint,” *Int. J. Press. Vessels Pip.*, vol. 88, no. 1, pp. 45- 56, 2011. DOI: 10.1016/j.ijpvp.2010.10.008.
51. O. Wiener, “Die Theorie des Mischkorpers für das Feld der stationären Stromung, Erste Abhandlung die Mittelwertsätze für Kraft,” *Polarisation und Energie Abh Math-Physichen Klasse Konigl Sacsh Gessel Wissen*, vol. 32, no. 6, pp. 509–604, 1912.

Table 1. Polymers and polymer blends composition and molding temperatures

| | | | | | | | |
|-------------------------------------|----------|----------|-----------|-------------------|--------------------|--------------------|------------------------------------|
| Polymer Composition (vol. %) | 100% PVC | 100% ABS | 100% HDPE | 50% PVC + 50% ABS | 50% PVC + 50% HDPE | 50% HDPE + 50% ABS | 33.3% PVC + 33.3% HDPE + 33.3% ABS |
| Processing temperature (°C) | 120 | 190 | 180 | 150 | 160 | 180 | 160 |

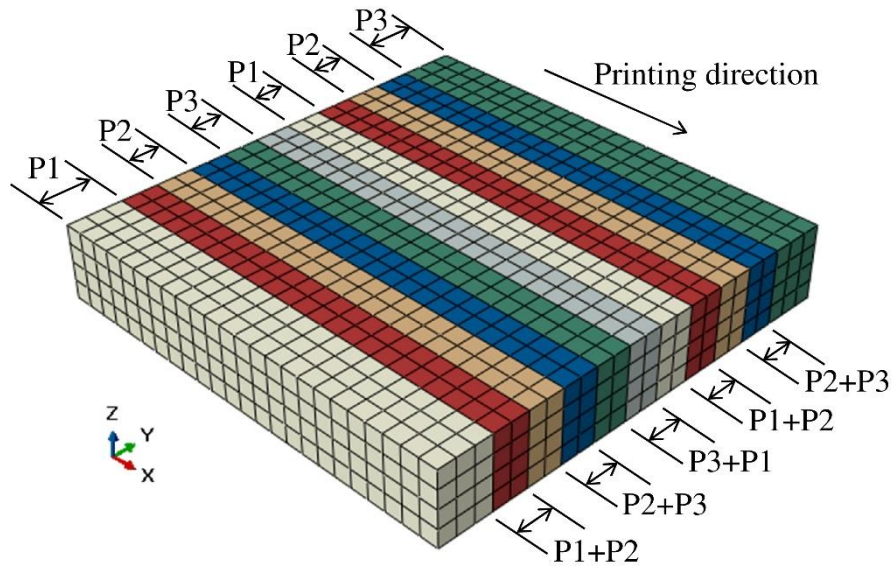


Figure 1. Generalized 3D model of layered polymer composite

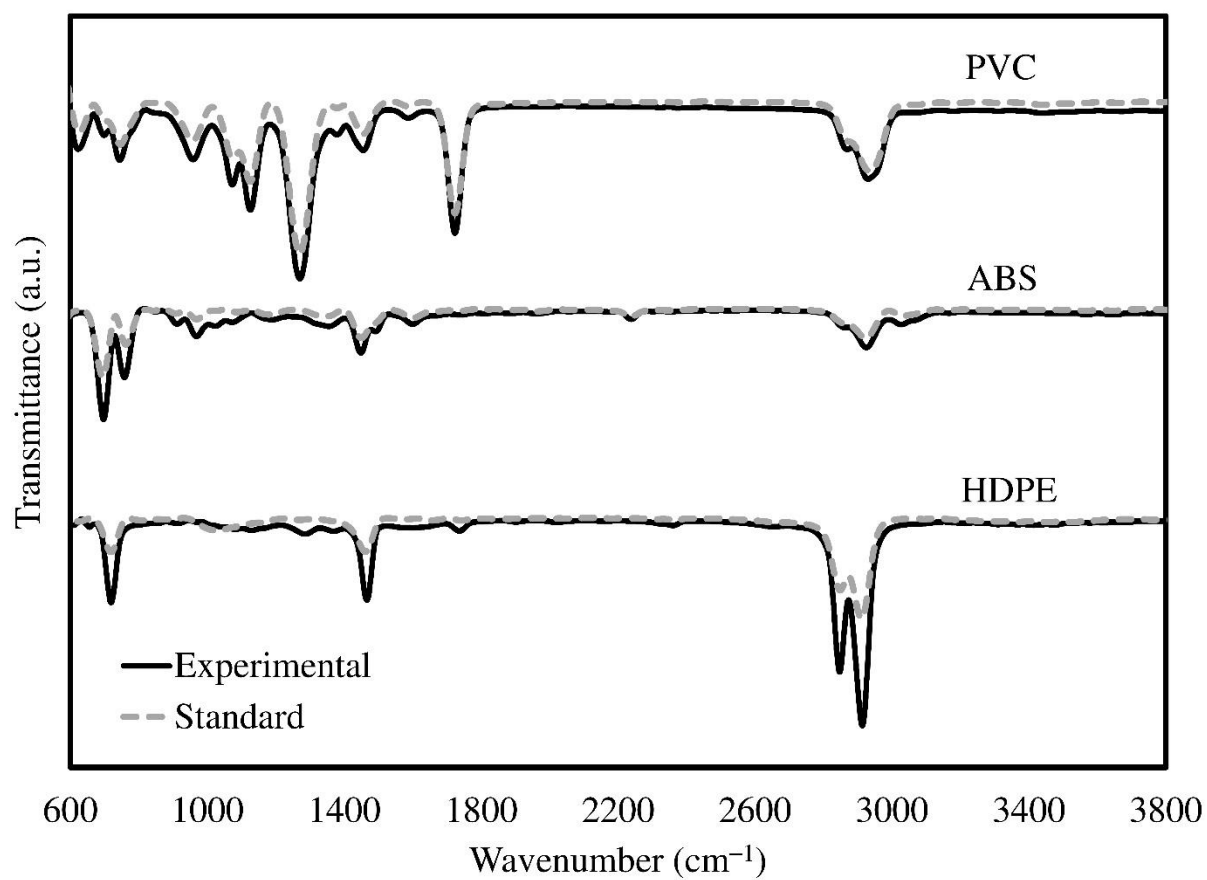


Figure 2. Comparison of standard and experimental FTIR curves of HDPE, ABS and PVC

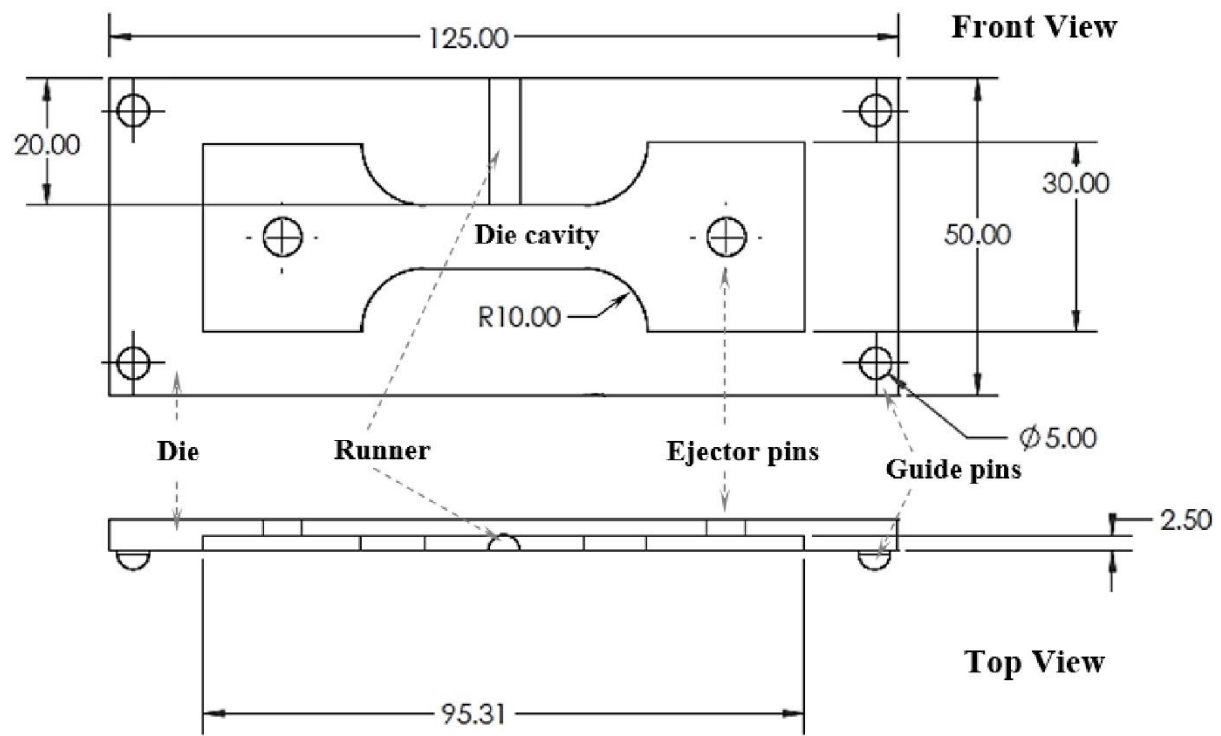


Figure 3. Injection molding die and tensile test specimen design (all dimensions are in mm)

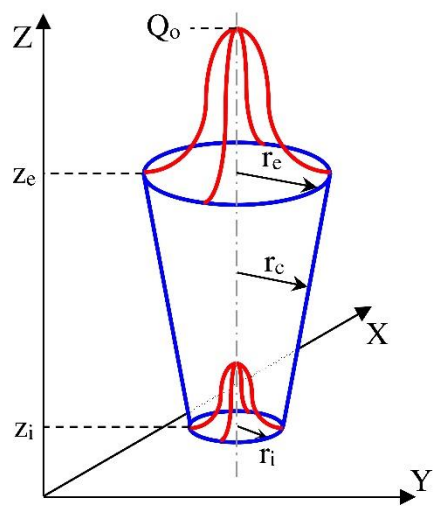


Figure 4. Conical volumetric heat source model with Gaussian distribution [49]

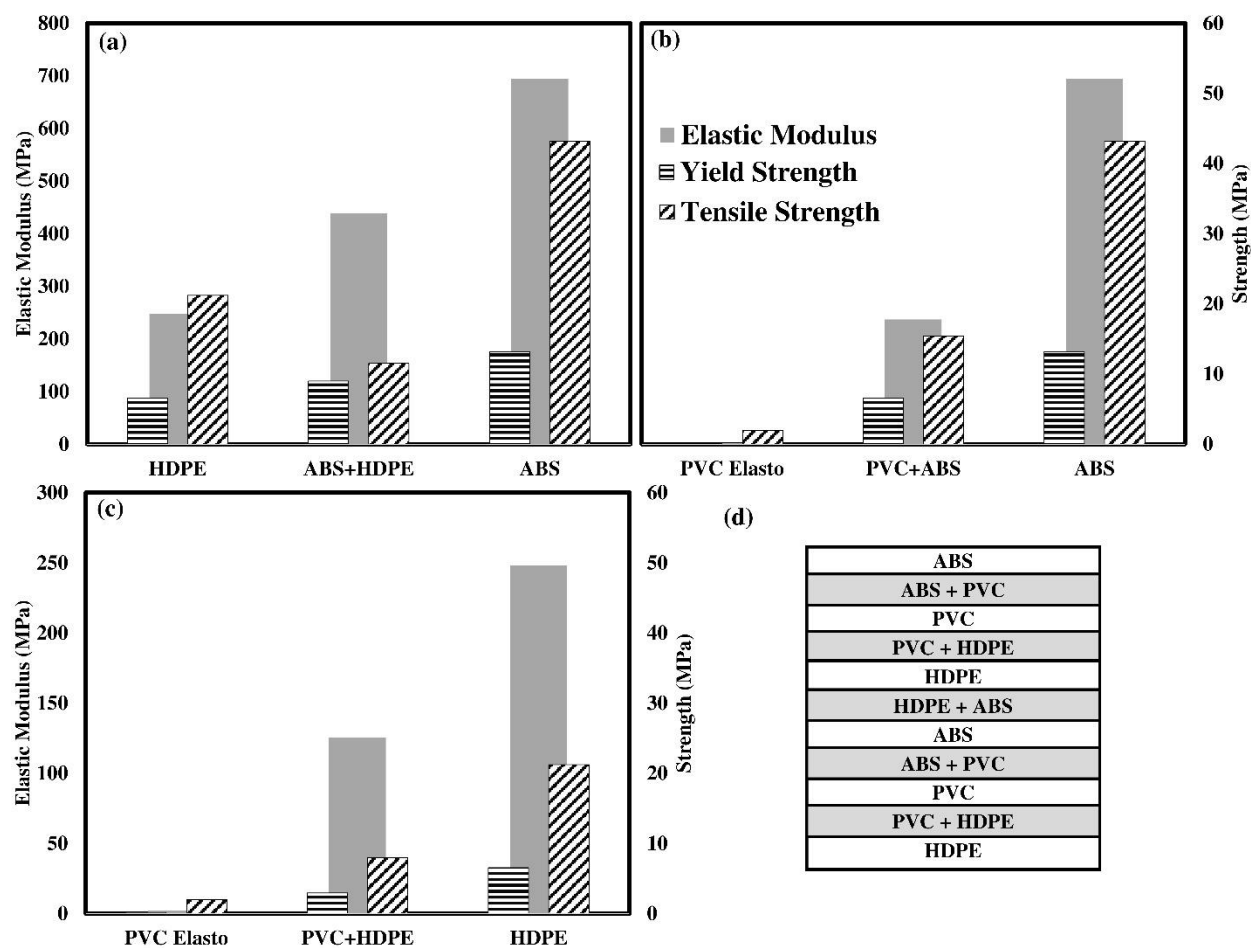


Figure 5. Comparison of mechanical properties of polymers: (a) HDPE, ABS, and 50 vol.% HDPE/50 vol.% ABS, (b) PVC, ABS, and 50 vol.% PVC/50 vol.% ABS, (c) HDPE, PVC, and 50 vol.% HDPE/50 vol.% PVC, (d) Sequence of the polymer layers and their interfaces

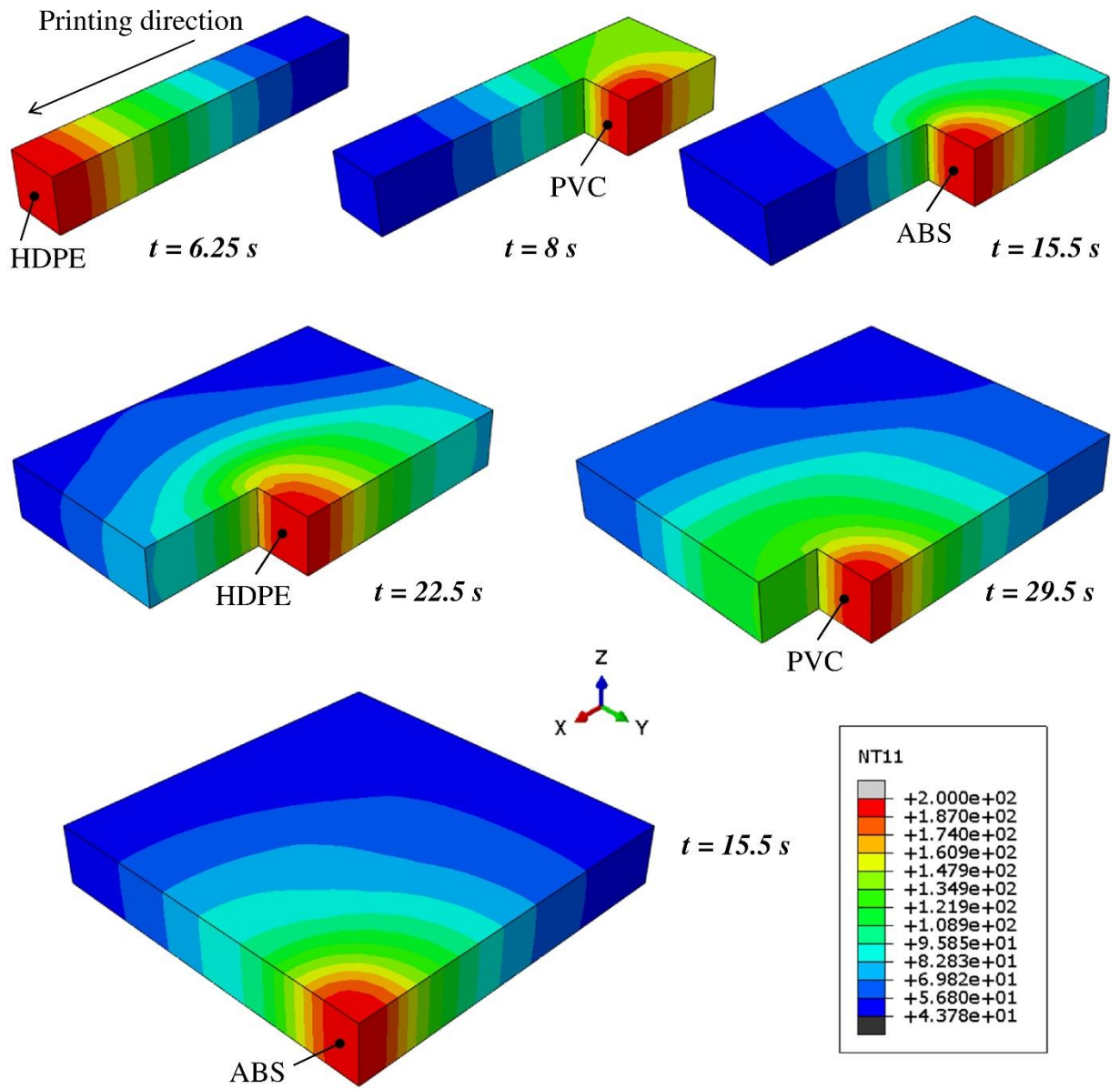


Figure 6. Temperature contours and element birth (activation) during 3D printing of polymer layered composite

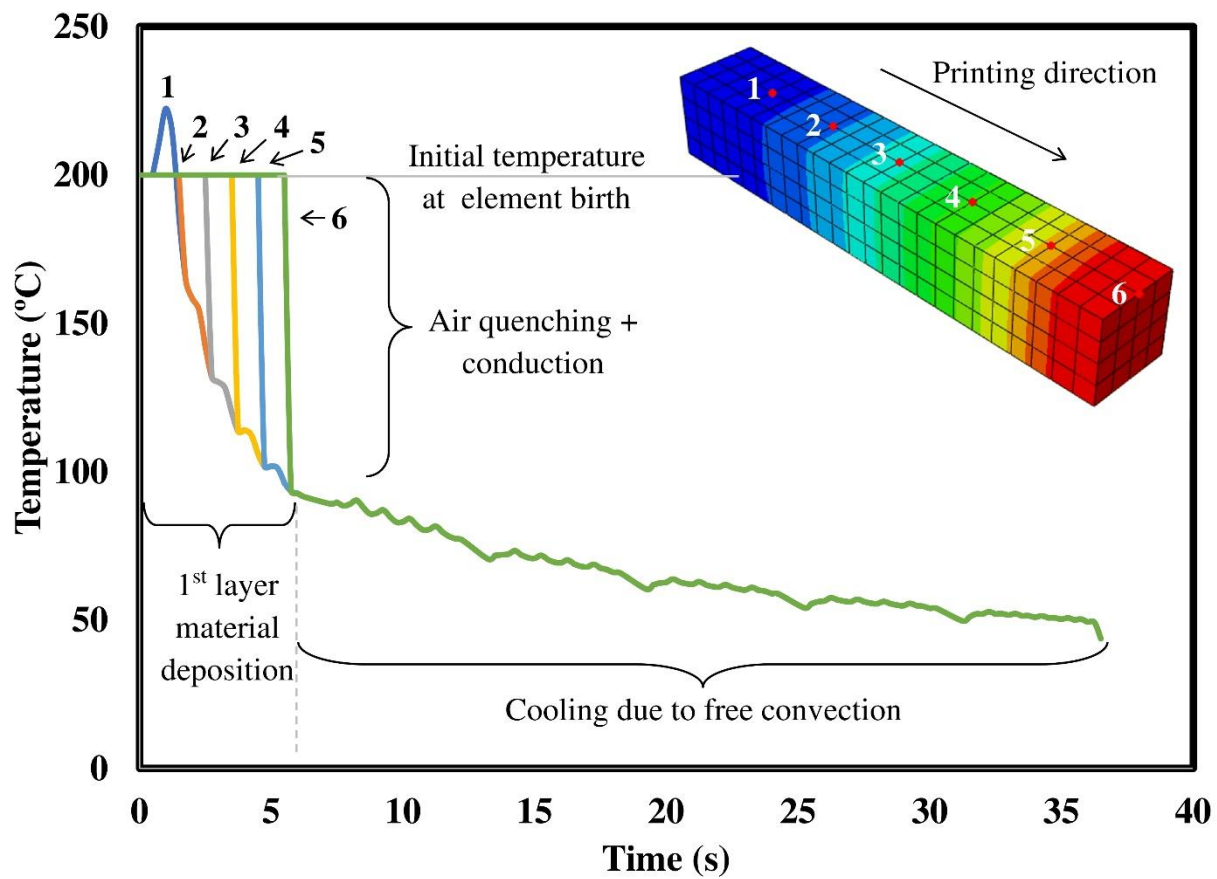


Figure 7. Temperature as a function of time graph for the deposition of first six element sets of HDPE

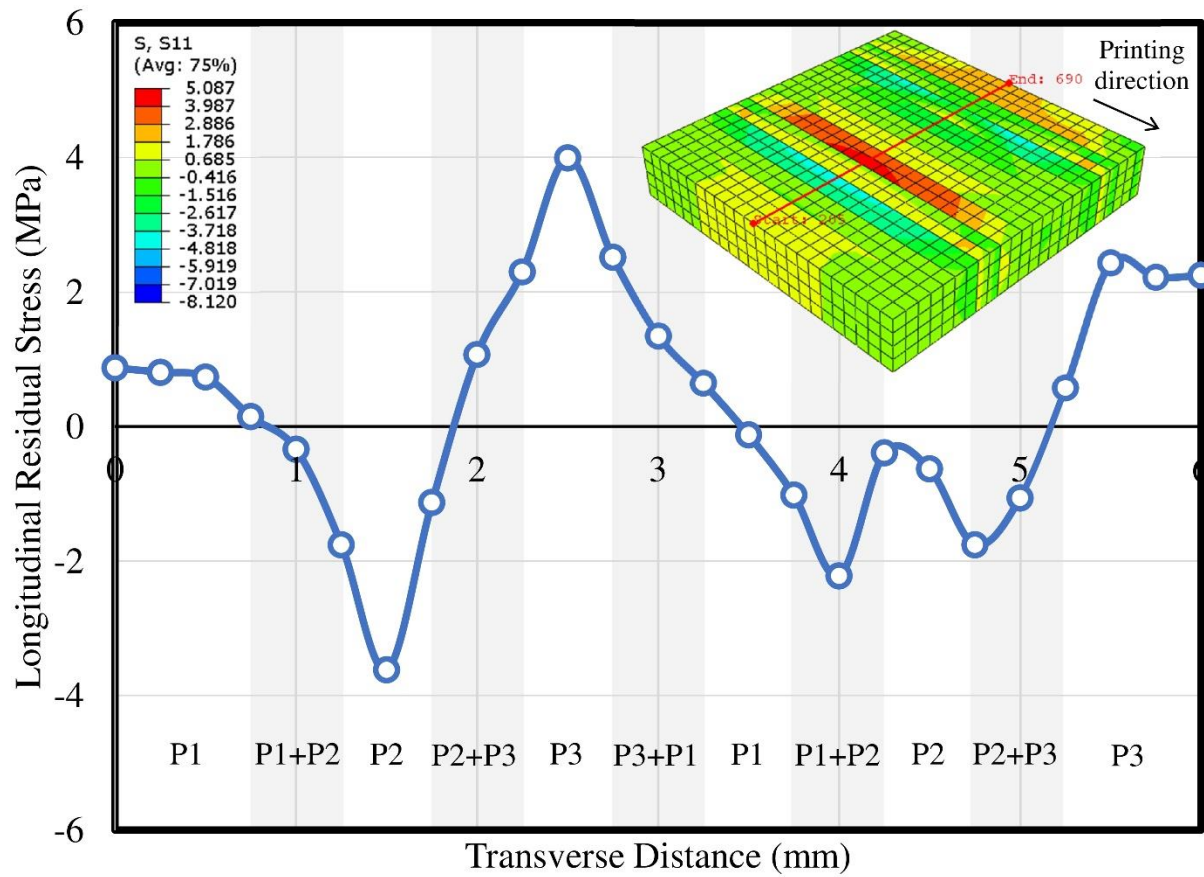


Figure 8. Longitudinal (along the print direction) residual stress contours and distribution as a function of transverse distance

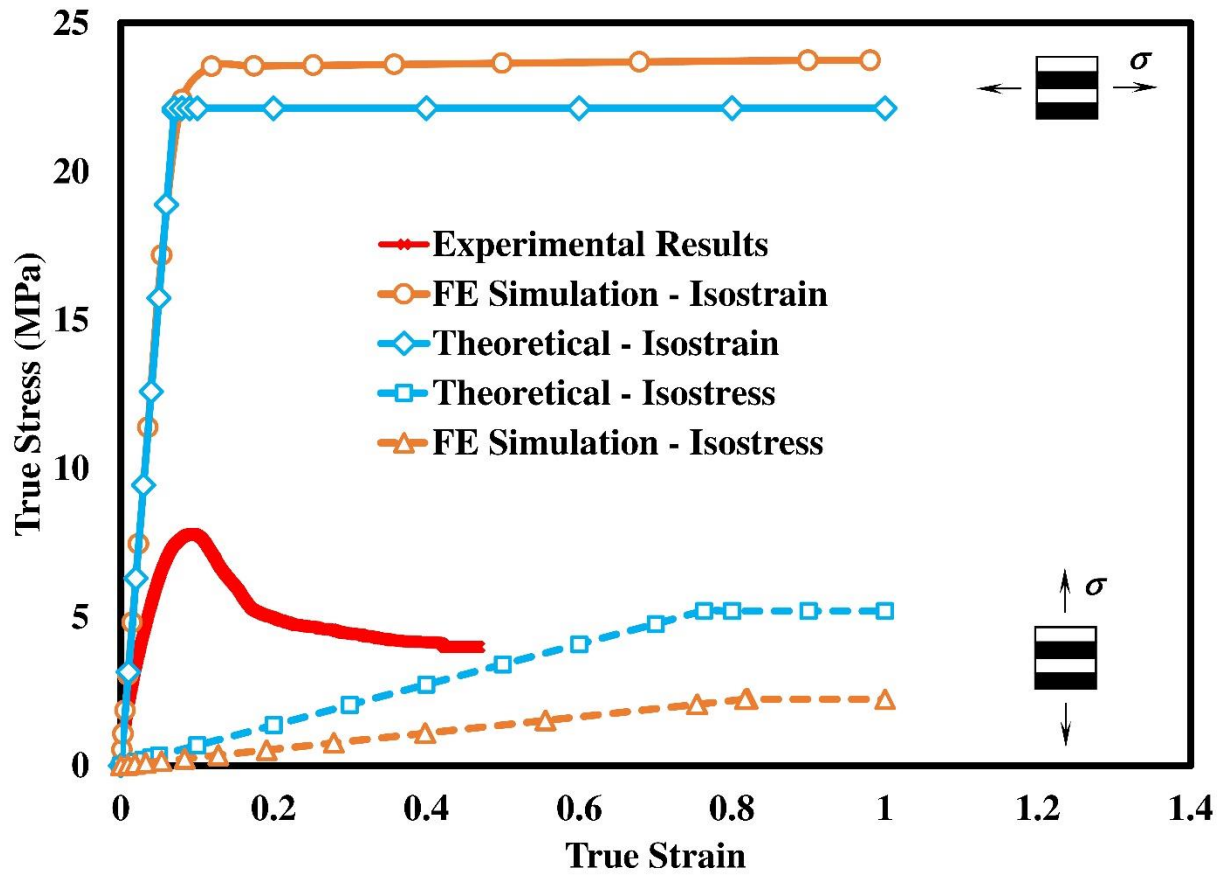


Figure 9. Comparison of experimental, FE simulation and theoretical true stress-true strain curves for equal volume fraction HDPE-PVC-ABS composite

List of Figure captions

Figure 1. Generalized 3D model of layered polymer composite.

Figure 2. Comparison of standard and experimental FTIR curves of HDPE, ABS and PVC

Figure 3. Injection molding die and tensile test specimen design (all dimensions are in mm)

Figure 4. Conical volumetric heat source model with Gaussian distribution [49]

Figure 5. Comparison of mechanical properties of polymers: (a) HDPE, ABS, and 50 vol.% HDPE/50 vol.% ABS, (b) PVC, ABS, and 50 vol.% PVC/50 vol.% ABS, (c) HDPE, PVC, and 50 vol.% HDPE/50 vol.% PVC, (d) Sequence of the polymer layers and their interfaces

Figure 6. Temperature contours and element birth (activation) during 3D printing of polymer layered composite

Figure 7. Temperature as a function of time graph for the deposition of first six element sets of HDPE

Figure 8. Longitudinal (along the print direction) residual stress contours and distribution as a function of transverse distance

Figure 9. Comparison of experimental, FE simulation and theoretical true stress-true strain curves for equal volume fraction HDPE-PVC-ABS composite